Title: Multifunctional polymerization domains determine the onset of epigenetic silencing in Arabidopsis

Authors: Anna Schulten[1], Geng-Jen Jang[1], Alex Payne-Dwyer[2,3], Mathias L. Nielsen[1,†], Mariann Bienz[4], Mark C. Leake[2,3], Caroline Dean[1,4*]

Affiliations:

[1]Department of Cell and Developmental Biology, John Innes Centre; Norwich, United Kingdom.

[2]School of Physics, Engineering and Technology, University of York; York, United Kingdom.

[3]Department of Biology, University of York; York, United Kingdom.

[4] Medical Research Council Laboratory of Molecular Biology; Cambridge, United Kingdom.

†Present address: Department of Immunology and Regenerative Biology, Weizmann Institute of Science; Rehovot, Israel.

*Corresponding author. Email: caroline.dean@jic.ac.uk

Abstract: Polycomb silencing at Arabidopsis *FLOWERING LOCUS C* (*FLC*) requires the accessory proteins VIN3 and VRN5. These interact via head-to-tail polymerization domains and are proposed to recruit and maintain Polycomb Repressive Complex 2 at the *FLC* nucleation region. Here, we show that VIN3 VEL polymerization is necessary *in vivo* for higher order nuclear VIN3 assemblies, strong chromatin association and efficient H3K27me3 nucleation. However, these are not dependent on the VRN5 VEL domain, despite its role in physically connecting VIN3 with the PRC2 complex. Because the VEL domain of VRN5 is also unable to functionally replace VIN3 VEL *in vivo*, this work defines a distinct role for VIN3 polymerization in the establishment of a chromatin environment promoting nucleation and the switch to an epigenetically silenced state.

Main Text:

The activity of the Polycomb Repressive Complex 2 (PRC2) is essential for the deposition of H3K27me3 as one of the hallmarks of mitotically inheritable gene silencing. Since the first identification of *cis*-regulatory Polycomb Response Elements (PREs) in Drosophila, a complex picture has emerged in which non-sequential multifactorial protein interactions with the local chromatin environment, also shaped by transcriptional activity, give rise to genome-wide Polycomb silencing patterns (*1-4*). Accessory proteins that interact with the highly conserved PRC2 core complex crucially define PRC2 subcomplexes with different activities and genomic enrichment sites (*5-10*). These mediate nucleation of Polycomb complexes and are required to maintain the Polycomb silenced state through cell division (*10-12*). However, it is still unclear how accessory protein function facilitates the digital switch to an epigenetically stable state and ensures inheritance of the silenced state to daughter cells during DNA replication.

In the model plant *Arabidopsis thaliana*, proteins of the VEL family (VIN3, VRN5 and VEL1) have been identified as accessory proteins to a PRC2 complex with the core subunit VRN2 (one of three homologs of mammalian SUZ12) (*13, 14*). Their genome-wide localization suggests a widespread role in PRC2 silencing of many loci in the Arabidopsis genome (*14*). Except for VEL1, their function is essential for the epigenetic silencing of the floral repressor gene *FLOWERING LOCUS C* (*FLC)* during the winter cold, a process called vernalization (*15-18*). At *FLC*, Polycomb silencing initiates via cold-induced nucleation of H3K27me3 over a

small number of nucleosomes around the first exon-intron boundary of *FLC*. This confers metastable epigenetic silencing that holds the silent state for tens of cell cycles (*19*). The metastable state is converted into a long-term epigenetically silenced state through the spreading of H3K27me3 across the *FLC* gene body, which occurs when the plants start to grow more rapidly following the return to ambient temperatures (*20*). Nucleation, which is strongly reduced in *vin3*, *vrn5* and *vrn2* single mutants, can be separated from the stable spread H3K27me3 state in mutants defective in one of the PRC2 methyltransferases genes *CURLY LEAF* (*CLF*), or *LIKE HETEROCHROMATIN PROTEIN 1* required to maintain long-term silencing (*21*). Studies in these mutants have shown that VEL proteins promote the stochastic PRC2-mediated nucleation of individual *FLC* alleles, whereby the fraction of nucleated *FLC* loci increases over prolonged cold of winter (*22*). In other words, the slow accumulation of H3K27me3 at the 3-4 nucleosome nucleation region is the result of a low probability digital ON/OFF switch, which occurs independently at each allele (*20, 23*).

A key question was: which features of the VEL proteins confer the ability to aid PRC2 engagement with these local sites, and to maintain epigenetic silencing through cell division? The VEL proteins share a domain architecture consisting of a tripartite plant homeodomain (PHD) superdomain, a fibronectin type III (FNIII) domain and a C-terminal VEL domain (*24, 25*) (Fig. 1A). Early data assumed they may be functionally similar, with one protein being cold-induced (VIN3) and the others (VRN5, VEL1) constitutively expressed (*15*). However, recent structural analysis has revealed that specifically in VRN5 there is a close packing of the central PHD superdomain and FNIII domain and this mediates its interaction with the PRC2 core complex. In contrast, VIN3 has a more open conformation of these domains and depends on VRN5 to interact with PRC2 (*14*).

The VEL domain mediates homo- and heterotypic interactions between the VEL proteins. Structural and functional analyses of the VEL domain revealed it to be a head-to-tail polymerization domain, conserved through the green lineage (*26*). It is only the third head-to-tail polymerization domain described in biology to date, their discovery often hindered by the insolubility of protein polymers in solution (*27*). We found that the spontaneous homo-polymerization of VIN3 and VEL1 via their VEL domains drives their assembly into dynamic biomolecular condensates detected by confocal microscopy following protein expression in heterologous systems (*26*). Mathematical modelling of epigenetic state switching and memory at *FLC* had predicted the requirement of additional protein memory storage elements that positively feedback to reinforce themselves; for example, molecular assemblies that are maintained in sufficiently high numbers to overcome the nucleation threshold and that may persist at the locus even through the nucleosome perturbations that occur during DNA replication (*19*). Nuclear assemblies of VEL proteins increase in stoichiometry during vernalization (*28*), so that VEL-dependent protein polymerization and condensate formation could provide such a mechanism. Here, we therefore experimentally tested the importance of the VEL polymerization domain in the switch to the epigenetically silenced state.

Contrasting PRC2-related phenotypes in VIN3 and VRN5 VEL domain mutants

We had previously shown that stable Arabidopsis lines expressing VIN3-GFP with single amino acid polymerization blocking point mutations located in the head and tail of the VEL domain (R556D/I575D [RI>DD], Fig. 1A), fail to rescue impaired *FLC* silencing in the *vin3* mutant (*26*). This pointed to the importance of polymerization in *FLC* silencing. To extend these findings we directly compared the effect of VIN3-GFP wild-type (WT) and RI>DD transgenes

when expressed at endogenous levels. Two homozygous single insertion lines with protein levels equal to a single-insertion VIN3-GFP WT line were selected from a larger T2 generation, all displaying the same non-complementation phenotype (Fig. S1). These VIN3-GFP RI>DD lines mirrored the impaired *FLC* shutdown during cold and the post-cold *FLC* reactivation observed for lines with a deletion of the entire VEL domain in VIN3-GFP (Fig. 1B and Fig. S1). Besides, H3K27me3 failed to accumulate at the *FLC* nucleation region in VIN3-GFP RI>DD (Fig. 1C). Because the RI>DD mutation disrupts VIN3 polymerization with minimal impact on the rest of the protein, we conclude that the polymerization of the VIN3 VEL domain is required to promote PRC2-mediated deposition of H3K27me3 in the *FLC* nucleation region.

Our prediction from the heterotypic interactions observed between VIN3 and VRN5 was that the VEL domain would be required for silencing by mediating the VRN5-dependent interaction between VIN3 and PRC2 (*14, 15*). However, independent homozygous stably transformed Arabidopsis VRN5-SYFP2 ΔVEL lines with single transgene insertions in a *vrn5* mutant background (Fig. 1A and Fig. S2) showed an unexpected result; *FLC* was fully silenced in VRN5-SYFP2 ΔVEL like in a *vrn5* rescue line expressing VRN5-SYFP2 WT (Fig. 1B). In agreement, the deposition of H3K27me3 at the *FLC* nucleation region was not impaired in VRN5 ΔVEL plants (Fig. 1D).

To further understand the different phenotypes observed for the VEL domain deletions of VIN3 and VRN5 *in vivo,* we determined the interaction partners of VIN3 and VRN5 dependent on the VEL domain. Native GFP co-immunoprecipitation (coIP) followed by mass spectrometry was undertaken with respective WT and ΔVEL seedlings vernalized for six weeks. Both VIN3 and VRN5 WT proteins co-precipitated all components of one of the Arabidopsis PRC2 core complexes (VRN2, FIE, MSI1, SWN and to a lesser extent CLF) as well as each other and VEL1 as expected (Fig. 1D). The deletion of the VIN3 VEL domain resulted in the loss of all PRC2 core subunits and VRN5/VEL1. Probing for the PRC2 subunit FIE with immunoblot analysis after coIP in extracts of vernalized plants confirmed the loss of FIE interaction in both VIN3 ΔVEL and VIN3 RI>DD lines (Fig. 1E). In contrast, the interaction with PRC2 was maintained in VRN5 ΔVEL plants (Fig. 1D). This is in accordance with our previous results from heterologous coIPs in mammalian cells which mapped the PHD superdomain and the FNIII of VRN5, but not the VEL domain to the interface for PRC2 interaction (*14*). Surprisingly, the interaction of VRN5 ΔVEL with VEL1 was also maintained, whereas the co-enrichment of VIN3 was strongly reduced. Although VEL1 has the same open conformation of the PHD superdomain and the FNIII domain as VIN3, it does interact specifically with the PRC2 core subunit MSI1 and this may explain the association with VRN5 ΔVEL (*14*). It remains unclear whether VEL1 function might also contribute to the rescue of *FLC* silencing observed in VRN5 ΔVEL lines.

Role of VEL domain in nuclear assembly formation of VIN3 and VRN5

The protein assemblies predicted to be involved in Polycomb epigenetic switching could be realised by VEL polymerization-based assemblies or by multimeric assemblies mediated by other interactors such as PRC2 (or combinations thereof). We therefore used the stable Arabidopsis transgenic VIN3-GFP and VRN5-SYFP2 lines to investigate the effects of VEL domain disruptions on the stoichiometry of both VIN3 and VRN5 in molecular assemblies *in vivo*. We performed single-particle tracking of the fluorescently tagged proteins with SlimVar microscopy, which uses an oblique illumination for rapid, enhanced imaging contrast enabling single-molecule detection sensitivity in intact root tips (*28*). Stepwise photobleaching is

133 employed as a calibration to determine the number of tagged molecules in detected
134 fluorescent particles (*29*).
135
136 In roots of seedlings vernalized for six weeks, we observed that the VIN3-GFP RI>DD
137 mutations resulted in VIN3 assemblies with lower number of molecules, only 29% of tracks
138 corresponded to assemblies larger than 10 molecules compared to 46% in VIN3-GFP WT
139 (Fig. 2A). For VRN5-SYFP2 ΔVEL, we observed an increase in stoichiometry in comparison
140 to the WT in seedlings vernalized for six weeks (Fig. 2B, for other time points see Fig. S3), in
141 contrast to the decrease expected if the assemblies were VEL-mediated. Based on the track
142 stoichiometry distribution, we calculated the periodicity, *i. e.* the intervals between nearest-
143 neighbour peaks, of VIN3 and VRN5 within the assemblies as a proxy for their internal order.
144 VIN3-GFP WT and VRN5-SYFP2 WT consistently showed dimeric units, which were disrupted
145 in VIN3-GFP RI>DD (Fig. 2C) but generally maintained for VRN5-SYFP2 ΔVEL (Fig. 2D).
146 Notably, we have previously observed VIN3 VEL domain crystals composed of protofilaments
147 with a dimeric unit; the result of a mutual domain swapping of VEL domain helices between
148 two VIN3 monomers (*26*). It remains to be determined whether PRC2 might also contribute to
149 VIN3 assembly formation during vernalization. Given the direct interaction between VRN5 and
150 PRC2, we speculate that VEL-independent dimeric periodicity of VRN5 may be a result of the
151 reported ability of PRC2 to undergo dimer formation (*30-32*).
152
153 Because we observed no reduction in the size of VRN5 assemblies and no effect on *FLC*
154 silencing in stable Arabidopsis lines carrying VRN5 ΔVEL, we questioned the properties of the
155 VRN5 VEL domain. VIN3 polymerization results in the formation of biomolecular condensates
156 (*26*), so we investigated VRN5 condensate formation after transient overexpression in leaf
157 epidermal cells of *Nicotiana benthamiana*. In comparison to the VEL- and polymerization
158 dependent discrete condensates formed by GFP-VIN3 (*26*), GFP-VRN5 formed much smaller
159 condensates, with more VRN5 protein diffusely distributed throughout the nucleus (Fig. 2E
160 and Fig. S4A, B). Upon expression in HeLa cells, GFP-VRN5 previously also appeared diffuse
161 (*26*). Tagging VRN5 with mScarlet gave the same result as observed for GFP-VRN5 in the *N.*
162 *benthamiana* system, where the deletion of the VRN5 VEL domain abolished the formation of
163 any discrete condensates (Fig. S4C-D). These observations are consistent with VRN5 having
164 a lower propensity to concentrate into condensates in a VEL-dependent manner. In agreement
165 with our *in vivo* coIP results, we observed the recruitment of mScarletI-VRN5 into GFP-VIN3
166 to form large condensates in the *N. benthamiana* system, a co-localization that was dependent
167 on the VRN5 VEL domain (Fig. 2F-H). Thus, the VRN5 VEL domain has some ability to homo-
168 and heteropolymerize but its properties appear different to the VEL domain of VIN3.
169
170 **VRN5 VEL domain is not functionally equivalent to VIN3 VEL**

171 To further examine the properties of the VRN5 VEL domain, we tested whether VRN5 VEL
172 can functionally replace VIN3 VEL in *FLC* silencing. A VIN3-GFP construct, in which the VIN3
173 VEL domain was replaced with the VRN5 VEL domain (Fig. 3A), was transformed into the *vin3*
174 mutant. *FLC* silencing during vernalization remained impaired in two independent
175 homozygous lines as well as in multiple other lines tested in the T2 generation (Fig. 3B and
176 Fig. S5). This suggests that VRN5 VEL is not functionally equivalent to VIN3. With equal VIN3
177 protein expression, coIP of the PRC2 subunit FIE was nearly undetectable in the VIN3-GFP
178 VRN5VEL line compared to VIN3-GFP WT (Fig. 3C), most likely caused by inefficient
179 interaction with endogenous VRN5. This result is consistent with reduced VRN5 condensate

formation in *N. benthamiana* cells (Fig. 2E). Equally, the heterologous co-expression of GFP-VIN3 VRN5VEL with mScarlet-VRN5 in these cells did not result in the formation of the large co-localized condensates that are observed upon co-expression of the wildtype proteins (Fig. 3D, S6). The experimentally determined structures of VIN3 and VEL1 VEL domains align closely with the Alphafold (AF) structure predictions (*26*) and comparing the latter to the AF prediction for the VRN5 VEL domain again shows a close superimposition (Fig. 3E). Thus, no major structural differences are predicted to underpin the functional differences between the VEL domains. Specific amino acid differences (either individual or combinations thereof), possibly associated with different post-translational modifications *in vivo*, may contribute to the functional differences between VIN3 and VRN5 VEL and deserve further investigation in the future (Fig. 3F). The residue $I575_{VIN3}/I664_{VEL1}$ in the VEL head interface engages in hydrophobic or electrostatic interactions with two basic residues in the complementary tail surface to mediate polymerization, blocked by the mutation I575D. A threonine in the corresponding position of Arabidopsis VRN5 (T565) and other VRN5 paralogs may be functionally significant as this is a polar hydrophilic rather than a hydrophobic amino acid (*26*).

VEL polymerization promotes multivalent VIN3 chromatin association independent of PRC2

To understand the specific contribution of VIN3 polymerization to *FLC* silencing, we determined whether the loss of interaction between VIN3 and PRC2 observed in the stable VIN3-GFP RI>DD, VIN3-GFP ΔVEL, VIN3-GFP *vrn5* as well as VIN3-GFP VRN5 VEL lines (Fig. 1D-E and Fig. 3C) would affect the association of VIN3 with the *FLC* locus. ChIP-qPCR experiments with vernalized seedlings revealed that VIN3-GFP *vrn5* and VIN3-GFP VRN5VEL showed equally high enrichment at *FLC* as VIN3-GFP WT (Fig. 4A and B), suggesting that the interaction between VIN3 and PRC2 is not *per se* required for VIN3 chromatin binding. In contrast, we observed a strongly reduced association of VIN3-GFP RI>DD and VIN3-GFP ΔVEL with the *FLC* nucleation region (Fig. 4C and S7A). The chromatin association of VRN5 ΔVEL at the *FLC* locus was WT-like in comparison (Fig. S7B). We also tested other VIN3 targets, previously identified by ChIP-seq experiments (*14*), and found reduced VIN3-GFP RI>DD association at several of these loci (Fig. S8). This implicates VEL-mediated polymerization in promoting and maintaining VIN3 chromatin association with *FLC* and other loci in a PRC2-independent manner.

An emerging paradigm for the function of head-to-tail protein polymerization is the increase in local concentration of polymerizing proteins and their ligand binding sites, which enhances their binding avidity for low-affinity ligands (functional affinity) (*27*). Because the head and tail interfaces of the VEL domain facilitates homo- and heterotypic interactions between the VEL proteins, both types of interactions can theoretically contribute to promote VIN3 chromatin association in such a mechanism. We observed that VIN3-GFP VRN5VEL does not restore the VRN5-dependent interaction with PRC2, yet it still binds to *FLC* efficiently; thus the properties of VIN3-VRN5VEL are sufficient for some but not all outputs achieved by the VIN3 WT protein and its VEL domain. This highlights the complexities at play *in vivo*.

We decided to test whether a functionally relevant binding site - whose avidity for its chromatin ligand might be enhanced by the VEL-dependent polymerization - is present in the VIN3 protein itself. We turned to the tripartite PHD superdomain of VIN3: although this domain is an atypical PHD domain in that it exhibits no histone H3 tail binding activity, it has a weak affinity for negatively charged DNA or RNA polymers *in vitro (25)*. We generated stable transgenic

225 Arabidopsis plants carrying VIN3-GFP with a deletion of the entire PHD superdomain
226 (ΔPHDsuper) in the *vin3* mutant background. The construct did not complement the *vin3*
227 mutant in *FLC* vernalization time course experiments in two homozygous lines or in multiple
228 other lines tested in the T2 generation (Fig. 4D and Fig. S9). While VIN3 ΔPHDsuper
229 maintained its interaction with PRC2 based on FIE immunoprecipitation in vernalized
230 seedlings (Fig. 4E), chromatin association with the *FLC* nucleation region was abolished (Fig.
231 4F). This demonstrates that the VIN3 PHD superdomain is necessary for chromatin
232 association and has chromatin or chromatin-associated ligands other than histone H3 tails.
233 Interestingly, H2A was among the significant VIN3 interactors identified by native coIP-MS
234 (Fig. 1D), more specifically the histone variant H2A.W which is known to associate with
235 H3K9me2-marked heterochromatin (*33*). For VIN3-GFP RI>DD, the binding peak at the *FLC*
236 nucleation region was much smaller than for VIN3-GFP WT but not entirely abolished (Fig.
237 4A). This may reflect the weak chromatin affinity of VIN3 monomers, mediated by the PHD
238 superdomain in the absence of the VIN3-mediated polymerization. These findings suggest
239 that VEL-mediated polymerization promotes a high local concentration of the VIN3 PHD
240 superdomain, enhancing its avidity for chromatin. Prolonged chromatin association of VIN3
241 would also increase PRC2 residence time, bridged by VRN5, to facilitate H3K27me3
242 nucleation. This is consistent with our previous observation that the *vin3* mutant, unlike *vrn5*,
243 accumulates the precursor mark H3K27me2 in the nucleation region, which suggested that
244 VIN3 is required to overcome the threshold from di- to trimethylation at *FLC (14)*.

245 That the VRN5 VEL domain is not essential for H3K27me3 nucleation suggests that the
246 association of the VIN3 polymer promotes H3K27me3 nucleation by other means in addition
247 to the recruitment of VRN5 and PRC2, eg. by modulating chromatin properties such as
248 nucleosome dynamics or by binding other protein factors. We previously found an interaction
249 between VIN3 and the transcriptional repressor VAL1, which serves as an assembly platform
250 for co-transcriptional repressors and chromatin regulators (*14, 34*). VAL1 binds to two RY-
251 motifs in the first *FLC* intron and would thus also provide a sequence-specific link to the *FLC*
252 locus (*35*). However, while transgenic Arabidopsis plants carrying a point mutation in the first
253 RY site (*FLC*-C585T) fail to nucleate H3K27me3, they still show an accumulation of
254 H3K27me2 specifically in the nucleation region, indicating that VAL1 is only one of the
255 multifactorial mechanisms that ensure targeting of VEL-PRC2 to this region (*14, 35*). In
256 agreement with this, we found that VIN3-GFP is still recruited to *FLC* in the C585T background
257 (Fig. S10). Overall, our findings for the VEL proteins have striking resemblance to a
258 polymerization network involving multiple Polycomb Repressive Complex 1 (PRC1) subunits
259 that engage in a combination of heterotypic and homotypic interactions to promote
260 transcriptional silencing in Drosophila. These interactions are mediated by the head-to-tail co-
261 polymerization of SAM domains of Polyhomeotic (Ph) and Sex combs of midleg (Scm) and
262 are linked to the Pho-repressive complex (PhoRC) subunit Sfmbt, which undergoes
263 heterotypic SAM interactions with Scm but is unable to homopolymerize (*36-38*). The DNA-
264 binding activity of the PhoRC complex contributes to this polymerization-mediated hub to
265 promote the nucleation of PRC1 complexes at target loci. SAM-containing Polycomb proteins
266 have not been found in plants (*39*), but VEL proteins may provide a mechanistically similar
267 function for PRC2.
268

269 **Conclusions**

270 In summary, we show that the PRC2 accessory protein VIN3 forms VEL polymerization-
271 dependent assemblies to promote PRC2-mediated deposition of H3K27me3 in the nucleation

region of *FLC*. While the VEL domain also mediates hetero-interaction between VIN3 and VRN5, linking VIN3 to the PRC2 complex, the VEL domain of VRN5 is not crucial for the nucleation activity of PRC2 and its properties are not sufficient to fully substitute for the function of the VIN3 VEL domain. We propose that polymerization via the VEL domain results in a high local concentration of VIN3 to promote its chromatin association, mediated by emergent multivalent interactions between VIN3 PHD superdomains and chromatin ligands. This would both facilitate recruitment of VRN5-PRC2 and potentially influence other local chromatin properties to overcome the nucleation threshold and promote H3K27me3 nucleation. Taken together, our work defines distinct roles for VEL polymerization in the digital switch to the Polycomb silenced state and extends our understanding of the principles that initiate epigenetic silencing.

References and Notes

1. A. Laugesen, J. W. Højfeldt, K. Helin, Molecular Mechanisms Directing PRC2 Recruitment and H3K27 Methylation. *Molecular Cell* **74**, 8-18 (2019).
2. D. Holoch *et al.*, A cis-acting mechanism mediates transcriptional memory at Polycomb target genes in mammals. *Nature Genetics* **53**, 1686-1697 (2021).
3. J. Déjardin *et al.*, Recruitment of Drosophila Polycomb group proteins to chromatin by DSP1. *Nature* **434**, 533-538 (2005).
4. J. Müller, J. A. Kassis, Polycomb response elements and targeting of Polycomb group proteins in Drosophila. *Current Opinion in Genetics & Development* **16**, 476-484 (2006).
5. G. van Mierlo, G. J. C. Veenstra, M. Vermeulen, H. Marks, The Complexity of PRC2 Subcomplexes. *Trends in Cell Biology* **29**, 660-671 (2019).
6. M. Perino *et al.*, Two Functional Axes of Feedback-Enforced PRC2 Recruitment in Mouse Embryonic Stem Cells. *Stem Cell Reports* **15**, 1287-1300 (2020).
7. D. T. Youmans, A. R. Gooding, R. D. Dowell, T. R. Cech, Competition between PRC2.1 and 2.2 subcomplexes regulates PRC2 chromatin occupancy in human stem cells. *Molecular Cell* **81**, 488-501.e489 (2021).
8. A. Petracovici, R. Bonasio, Distinct PRC2 subunits regulate maintenance and establishment of Polycomb repression during differentiation. *Molecular Cell* **81**, 2625-2639.e2625 (2021).
9. S. Chen, L. Jiao, M. Shubbar, X. Yang, X. Liu, Unique Structural Platforms of Suz12 Dictate Distinct Classes of PRC2 for Chromatin Binding. *Molecular Cell* **69**, 840-852.e845 (2018).
10. O. Oksuz *et al.*, Capturing the Onset of PRC2-Mediated Repressive Domain Formation. *Molecular Cell* **70**, 1149-1162.e1145 (2018).
11. R. T. Coleman, G. Struhl, Causal role for inheritance of H3K27me3 in maintaining the OFF state of a Drosophila HOX gene. *Science* **356**, eaai8236 (2017).
12. F. Laprell, K. Finkl, J. Müller, Propagation of Polycomb-repressed chromatin requires sequence-specific recruitment to DNA. *Science* **356**, 85-88 (2017).
13. F. De Lucia, P. Crevillen, A. M. Jones, T. Greb, C. Dean, A PHD-polycomb repressive complex 2 triggers the epigenetic silencing of FLC during vernalization. *Proc Natl Acad Sci U S A* **105**, 16831-16836 (2008).
14. E. Franco-Echevarría *et al.*, Distinct accessory roles of Arabidopsis VEL proteins in Polycomb silencing. *Genes & Development* **37**, 801-817 (2023).

15. T. Greb *et al.*, The PHD Finger Protein VRN5 Functions in the Epigenetic Silencing of Arabidopsis FLC. *Current Biology* **17**, 73-78 (2007).
16. S. Sung, R. M. Amasino, Vernalization in *Arabidopsis thaliana* is mediated by the PHD finger protein VIN3. *Nature* **427**, 159-164 (2004).
17. A. R. Gendall, Y. Y. Levy, A. Wilson, C. Dean, The VERNALIZATION 2 Gene Mediates the Epigenetic Regulation of Vernalization in Arabidopsis. *Cell* **107**, 525-535 (2001).
18. D.-H. Kim, S. Sung, The Plant Homeo Domain finger protein, VIN3-LIKE 2, is necessary for photoperiod-mediated epigenetic regulation of the floral repressor, MAF5. *Proceedings of the National Academy of Sciences* **107**, 17029-17034 (2010).
19. C. Lövkvist *et al.*, Hybrid protein assembly-histone modification mechanism for PRC2-based epigenetic switching and memory. *eLife* **10**, e66454 (2021).
20. H. Yang *et al.*, Distinct phases of Polycomb silencing to hold epigenetic memory of cold in Arabidopsis. *Science* **357**, 1142-1145 (2017).
21. J. S. Mylne *et al.*, LHP1, the Arabidopsis homologue of HETEROCHROMATIN PROTEIN1, is required for epigenetic silencing of *FLC*. *Proceedings of the National Academy of Sciences* **103**, 5012-5017 (2006).
22. A. Angel *et al.*, Vernalizing cold is registered digitally at *FLC*. *Proceedings of the National Academy of Sciences* **112**, 4146-4151 (2015).
23. S. Berry, C. Dean, M. Howard, Slow Chromatin Dynamics Allow Polycomb Target Genes to Filter Fluctuations in Transcription Factor Activity. *Cell Systems* **4**, 445-457.e448 (2017).
24. J. Mylne, T. Greb, C. Lister, C. Dean, Epigenetic Regulation in the Control of Flowering. *Cold Spring Harbor Symposia on Quantitative Biology* **69**, 457-464 (2004).
25. E. Franco-Echevarría, T. J. Rutherford, M. Fiedler, C. Dean, M. Bienz, Plant vernalization proteins contain unusual PHD superdomains without histone H3 binding activity. *J Biol Chem* **298**, 102540 (2022).
26. M. Fiedler *et al.*, Head-to-tail polymerization by VEL proteins underpins cold-induced Polycomb silencing in flowering control. *Cell Reports* **41**, (2022).
27. M. Bienz, Head-to-Tail Polymerization in the Assembly of Biomolecular Condensates. *Cell* **182**, 799-811 (2020).
28. A. L. Payne-Dwyer, G.-J. Jang, C. Dean, M. C. Leake, SlimVar: rapid *in vivo* single-molecule tracking of chromatin regulators in plants. *bioRxiv*, 2024.2005.2017.594710 (2024).
29. M. C. Leake *et al.*, Stoichiometry and turnover in single, functioning membrane protein complexes. *Nature* **443**, 355-358 (2006).
30. S. Chen, L. Jiao, X. Liu, X. Yang, X. Liu, A Dimeric Structural Scaffold for PRC2-PCL Targeting to CpG Island Chromatin. *Molecular Cell* **77**, 1265-1278.e1267 (2020).
31. D. Grau *et al.*, Structures of monomeric and dimeric PRC2:EZH1 reveal flexible modules involved in chromatin compaction. *Nature Communications* **12**, 714 (2021).
32. P. V. Sauer *et al.*, Activation of automethylated PRC2 by dimerization on chromatin. *bioRxiv*, 2023.2010.2012.562141 (2023).
33. Z. J. Lorković *et al.*, Compartmentalization of DNA Damage Response between Heterochromatin and Euchromatin Is Mediated by Distinct H2A Histone Variants. *Current Biology* **27**, 1192-1199 (2017).
34. P. Mikulski *et al.*, VAL1 acts as an assembly platform co-ordinating co-transcriptional repression and chromatin regulation at Arabidopsis FLC. *Nature Communications* **13**, 5542 (2022).

35. J. I. Qüesta, J. Song, N. Geraldo, H. An, C. Dean, Arabidopsis transcriptional repressor VAL1 triggers Polycomb silencing at *FLC* during vernalization. *Science* **353**, 485-488 (2016).
36. F. Frey *et al.*, Molecular basis of PRC1 targeting to Polycomb response elements by PhoRC. *Genes Dev* **30**, 1116-1127 (2016).
37. H. Kang *et al.*, Sex comb on midleg (Scm) is a functional link between PcG-repressive complexes in Drosophila. *Genes & Development* **29**, 1136-1150 (2015).
38. C. Alfieri *et al.*, Structural basis for targeting the chromatin repressor Sfmbt to Polycomb response elements. *Genes Dev* **27**, 2367-2379 (2013).
39. Y. Huang *et al.*, Evolution and conservation of polycomb repressive complex 1 core components and putative associated factors in the green lineage. *BMC Genomics* **20**, 533 (2019).
40. A. L. Payne-Dwyer, G.-J. Jang, C. Dean, M. C. Leake, SlimVar: rapid *in vivo* single-molecule tracking of chromatin regulators in plants. *bioRxiv*, 2024.2005.2017.594710 (2024).
41. L. Adler *et al.*, The role of BST4 in the pyrenoid of *Chlamydomonas reinhardtii*. *bioRxiv*, 2023.2006.2015.545204 (2023).

Acknowledgements

We thank Shuqin Chen and Caroline Smith for their excellent technical help. We are grateful to Gerhard Saalbach and Carlo Martin from the JIC proteomics facility for performing mass spectrometry analysis. We also thank all members of the Dean and Howard groups as well as Elsa Franco-Echevarría and Marc Fiedler for discussions.

Funding: This work was funded by the European Research Council Advanced Grant (EPISWITCH-833254), Wellcome Trust (210654/Z/18/Z), Biotechnology and Biological Sciences Research Council Institute Strategic Programmes (BB/J004588/1 and BB/P013511/1), EPSRC (EP/T00214X/1, EP/T002166/1 and EP/W024063/1) and a Royal Society Professorship (RP\R1\180002) to CD.

Author contributions: MB and CD conceived the study. AS, GJY, APD and MLN performed the investigation and analysed the data. AS and CD wrote the manuscript; all authors reviewed and edited the manuscript. MCL and CD supervised the study, acquired the funding, and were the project administrators.

Competing interests: Authors declare that they have no competing interests.

Data and materials availability: The mass spectrometry proteomics data have been deposited to the ProteomeXchange Consortium via the PRIDE partner repository with the dataset identifier PXD048844 and doi 10.6019/PXD048844. SlimVar microscopy data has been deposited to the BioStudies repository under the doi 10.6019/S-BIAD1233. All other microscopy data has been deposited to BioStudies under the doi 10.6019/S-BIAD1249.

Figure 1

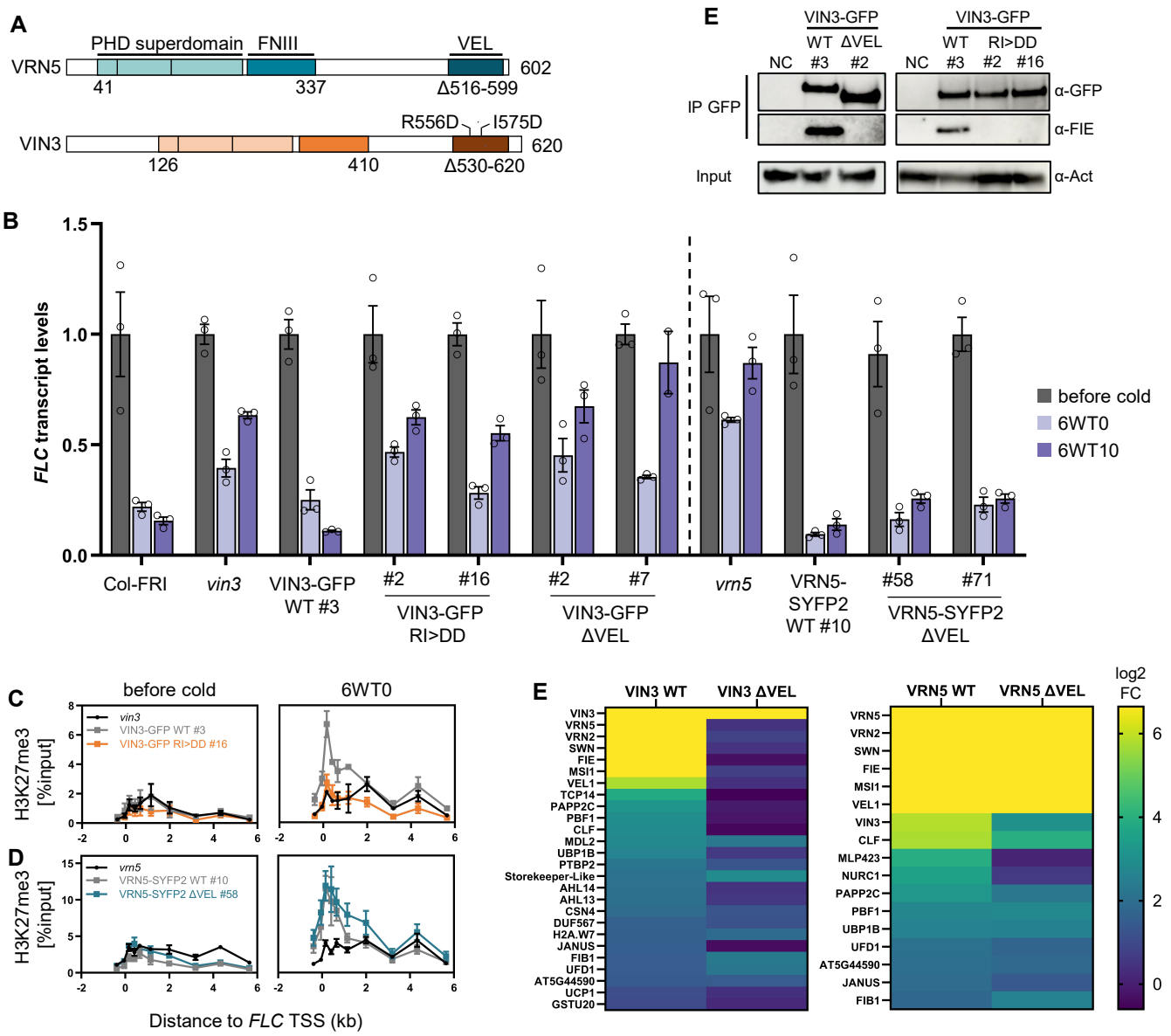

Fig. 1: VIN3 and VRN5 VEL domain mutant lines have contrasting phenotypes

(A) Domain architecture of VEL proteins VIN3 and VRN5. Tripartite PHD superdomain: a zinc finger, an atypical PHD domain and a four-helix bundle. Above: R556D and I575D indicate polymerization-blocking point mutations in VIN3 VEL; below: amino acids deleted in VIN3-GFP ΔVEL and VRN5-SYFP2 ΔVEL. (B) qRT-PCR assays of *FLC* transcripts during a vernalization timecourse; before cold, after 6-week cold exposure (6WT0), or 10 days post-cold (6WT10). Data are relative to the geometric mean of *UBC*/*PP2A*, normalized to *FLC* before cold. Error bars represent standard deviations (n = 3 biological replicates). (C) H3K27me3 ChIP across the *FLC* locus before cold and after 6-week cold, relative to input. TSS: transcriptional start site. Error bars represent SEM (n = 3 biological replicates). (D) Heatmap from IP-MS samples showing nuclear proteins co-precipitating with VIN3 and VRN5 baits in vernalized seedlings. log2 fold-change (FC) is in comparison to non-transgenic Col-FRI (adj. p-value ≤ 0.05 for wild-type proteins, n = 3 biological replicates). (E) Immunoblots of α-GFP immunoprecipitates using vernalized plants with VIN3-GFP transgenes, probed with α-FIE (PRC2 core). Non-transgenic Col-FRI was used as negative control (NC). Blots shown are representative of three replicates.

Figure 2

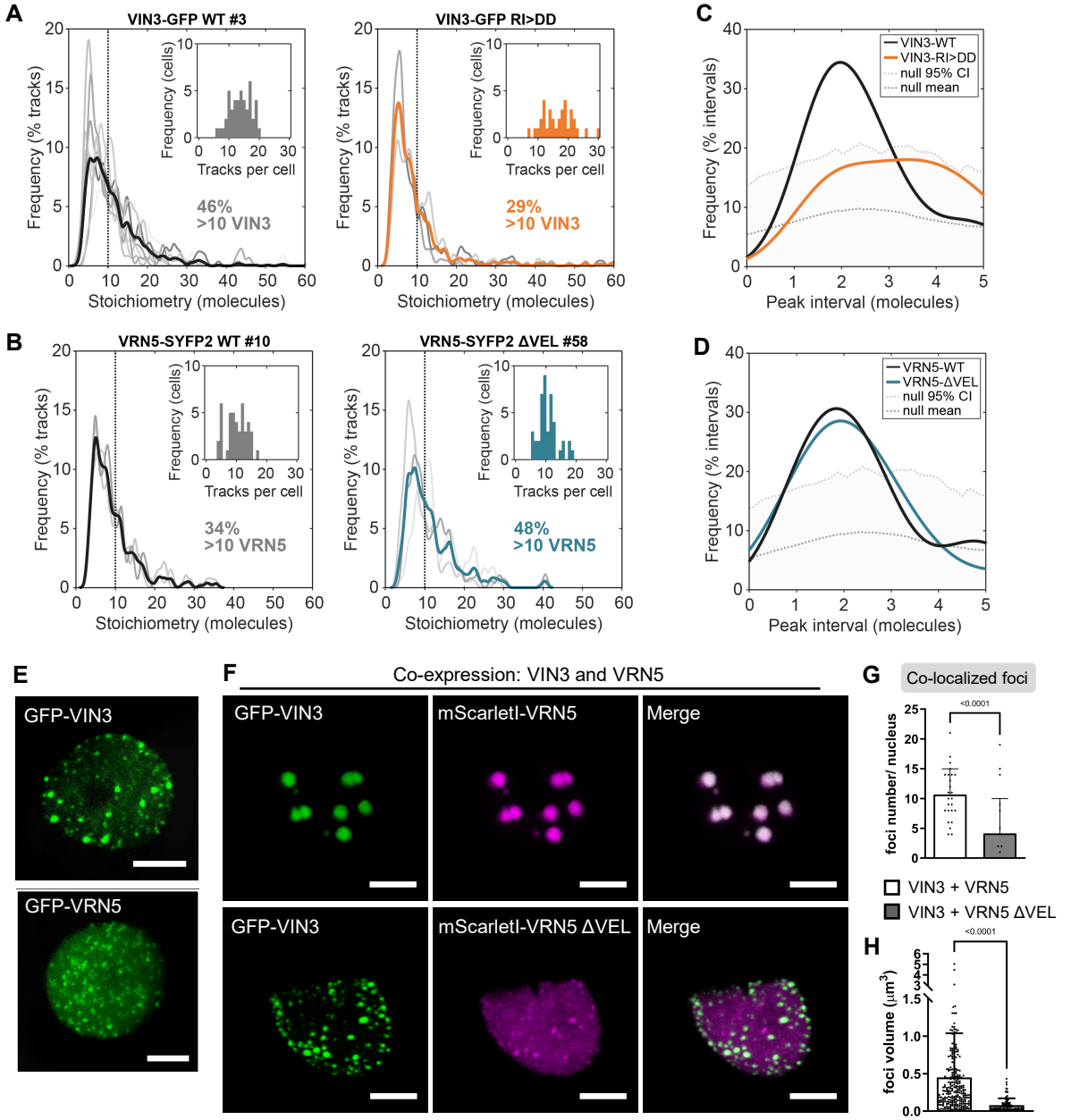

Fig. 2: VEL-dependent VIN3 and VRN5 assemblies in vivo and after transient heterologous expression

(A, B) Stoichiometry (molecule number) distributions of SlimVar tracked assemblies of (A) VIN3-GFP WT and VIN3-GFP RI>DD and (B) VRN5-SYFP2 WT and VRN5-SYFP2 ΔVEL in root nuclei of seedlings vernalized for 6 weeks. Individual replicates (*n* = 3-8 experiments, with 9-18 nuclei each) in grey, coloured line indicates mean distribution. Insets show the frequency of tracks per cell. Data collection statistics: Fig. S3. (C, D) Distributions of intervals between nearest neighbour stoichiometry peaks of tracked assemblies in (A, B). Upper dotted line indicates the null 95% confidence interval determined from simulations of random aperiodic stoichiometry, distributions which fall below are consistent with the null hypthesis (*28*). (E, F) Representative confocal images of epidermal leaf cell nuclei in *N. benthamiana,* (E) transiently expressing GFP-VIN3 or GFP-VRN5, and (F) transiently co-expressing GFP-VIN3 (green) and mScarlet-VRN5 (magenta) wild-type or mutant as indicated; scale bars 5 µm. (G, H) Quantification of number per nucleus (G) and volume of foci (H) observed in (F). Error bars represent standard deviation (*n* = 20-25 nuclei for (G) and *n* = 266 (VIN3 + VRN5) or 83 (VIN3 + VRN5 ΔVEL) foci for (H)).

Figure 3

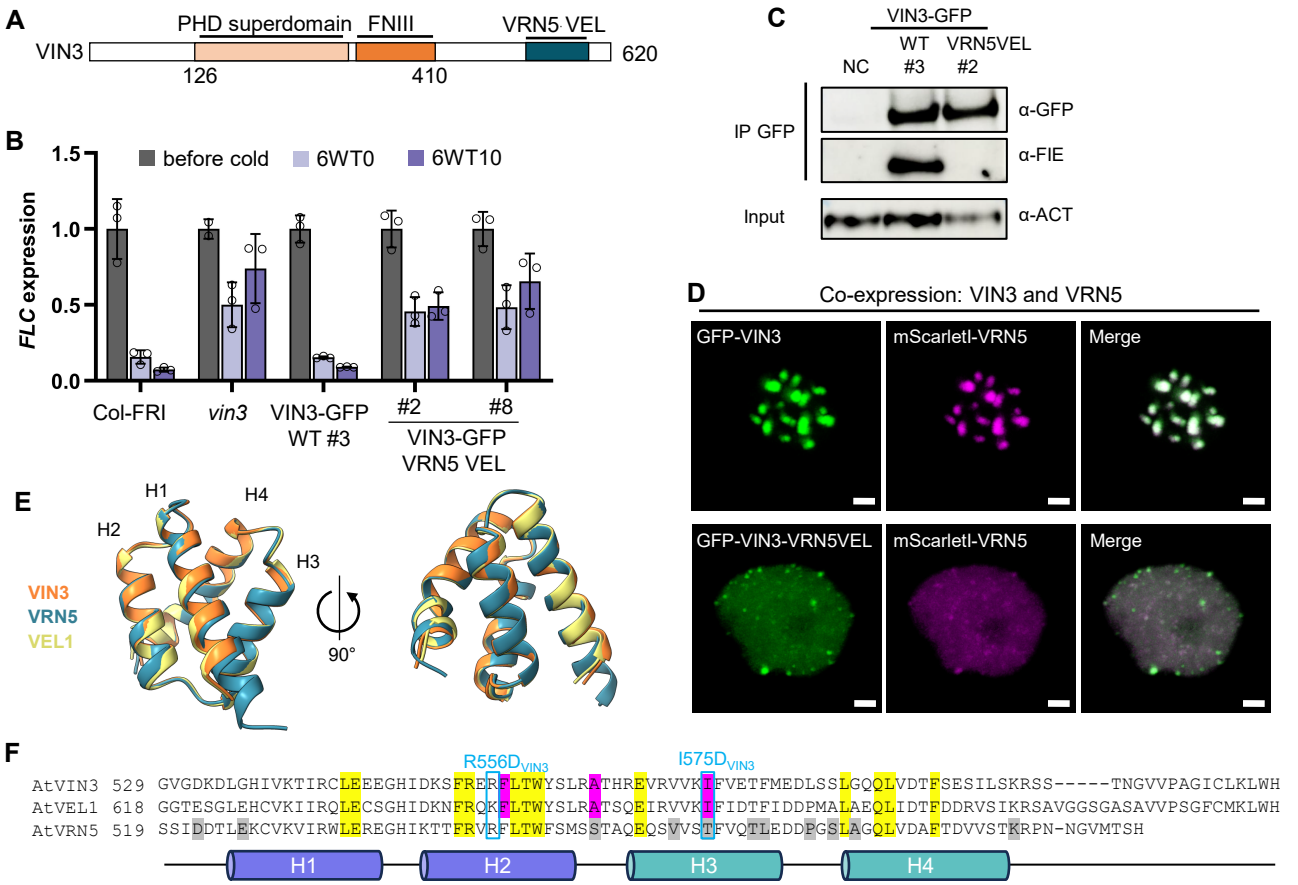

Fig. 3: VRN5 VEL cannot replace VIN3 VEL function in planta

(A) VIN3-GFP VRN5 VEL chimera construct transformed into the *vin3* mutant. (B) qRT-PCR assays of *FLC* transcripts during a vernalization timecourse; before cold, after 6-week cold exposure (6WT0), or 10 days post-cold (6WT10). Data are relative to the geometric mean of *UBC*/*PP2A*, normalized to *FLC* before cold. Error bars represent standard deviations (n = 3 biological replicates). (C) Immunoblots of α-GFP immunoprecipitates from vernalized plants with indicated VIN3-GFP transgenes, probed with α-FIE (PRC2 core). Non-transgenic Col-FRI was used as negative control (NC). Blots shown are representative of three replicates. (D) Representative confocal images of epidermal leaf cell nuclei in *N. benthamiana,* transiently co-expressing GFP-VIN3 or GFP-VIN3 VRN5 VEL (green) and mScarlet-VRN5 (magenta); scale bars 2 µm. (E) Superpositions of VEL domains of Arabidopsis $VRN5_{515\text{-}592}$ (teal), $VIN3_{529\text{-}601}$ (orange) and $VEL1_{618\text{-}690}$ (yellow) as predicted by Alphafold. VIN3 and VEL1 AF predictions superpose closely with experimentally determined structures (*26*). (F) Sequence alignment of Arabidopsis VEL domains from *VIN3, VRN5 and VEL1*. α-helices are indicated underneath; above, VIN3 mutations that block self-association. Coloured residues are conserved in angiosperm VELs (yellow), in VRN5 paralog VELs (grey) or in VIN3/VEL1 paralog VELs (pink).

Figure 4

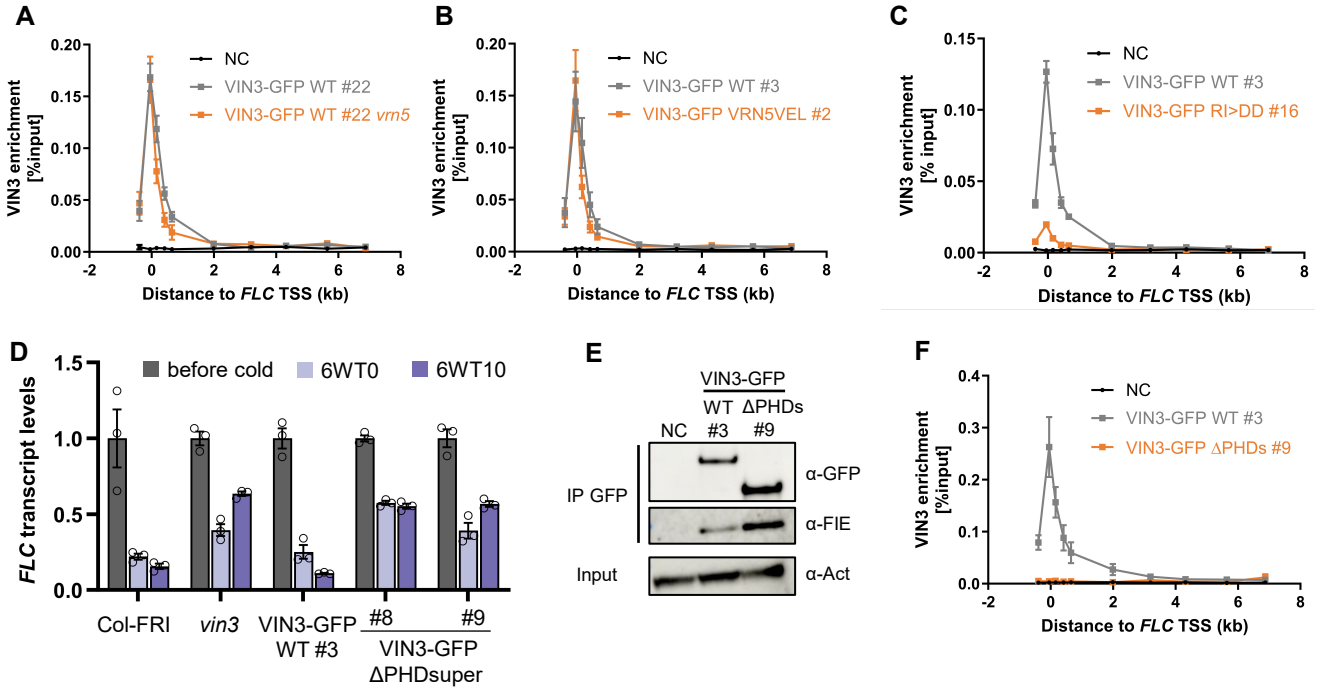

Fig. 4: VIN3 chromatin association is promoted by VEL-mediated polymerization and chromatin binding of the PHD superdomain

(A-C, F) ChIP-qPCR showing enrichment of VIN3-GFP (wildtype or mutant as indicated) across the *FLC* locus in seedlings vernalized for 6 weeks. Non-transgenic Col-*FRI* plants were used as negative control sample (NC). Data are relative to input control, error bars represent SEM (n = 2-4). (D) qRT-PCR assays of *FLC* transcripts during a vernalization timecourse; before cold, after 6-week cold exposure (6WT0), or 10 days post-cold (6WT10). Data are relative to the geometric mean of *UBC*/*PP2A*, normalized to *FLC* before cold. Error bars represent standard deviations (n = 3 biological replicates). (E) Immunoblots of α-GFP immunoprecipitates from extracts of vernalized plants bearing the indicated VIN3-GFP transgenes, probed with α-FIE (PRC2 core subunit) antibody. Non-transgenic Col-FRI was used as a negative control (NC). Blots shown are a representative of three replicates.